Decay of Cystalline Order and Equilibration during the Solid-to-Plasma Transition Induced by 20-fs Microfocused 92-eV Free-Electron-Laser Pulses

E. Galtier and F. B. Rosmej*
Sorbonne Universités, Pierre et Marie Curie, UMR 7605, LULI, case 128, 4 Place Jussieu, F-75252 Paris Cedex 05, France

T. Dzelzainis and D. Riley
School of Mathematics and Physics, Queens University Belfast, Belfast BT7 1NN, United Kingdom

F. Y. Khattak
Department of Physics, Kohat University of Science and Technology, Kohat 26000, Khyber Pakhtunkhwa, Pakistan

P. Heimann
Lawrence Berkeley National Laboratory, 1 Cyclotron Road Berkeley California 94720 USA

R. W. Lee and A. J. Nelson
Lawrence Livermore National Laboratory, Livermore California 94551 USA

S. M. Vinko, T. Whitcher, and J. S. Wark
Department of Physics, Clarendon Laboratory, Parks Road, University of Oxford, OX1 3PU, United Kindom

T. Tschentscher
European XFEL, Albert-Einstein-Ring 19, 22761 Hamburg, Germany

S. Toleikis and R. R. Fäustlin
Deutsches-Elektronensynchrotron DESY, Notkestrasse 85, 22603 Hamburg, Germany

R. Sobierajski
FOM-Institute for Plasma Physics, Rijnhuizen, Edisonbaan 14, NL-3430 BE Nieuwegein, The Netherlands

M. Jurek
Institute of Physics, Polish Academy of Sciences, Aleja Lotników 32/46, PL-02-668 Warsaw, Poland

L. Juha, J. Chalupsky, V. Hajkova, and M. Kozlova
Institute of Physics ASCR, Na Slovance 2, 182 21 Prague 8, Czech Republic

J. Krzywinski and B. Nagler
SLAC National Accelerator Laboratory, 2575 Sand Hill Road, Menlo Park, California 94025 USA
(Received 24 August 2010; published 18 April 2011)

We have studied a solid-to-plasma transition by irradiating Al foils with the FLASH free electron laser at intensities up to 10^{16} W/cm^2. Intense XUV self-emission shows spectral features that are consistent with emission from regions of high density, which go beyond single inner-shell photoionization of solids. Characteristic features of intrashell transitions allowed us to identify Auger heating of the electrons in the conduction band occurring immediately after the absorption of the XUV laser energy as the dominant mechanism. A simple model of a multicharge state inverse Auger effect is proposed to explain the target emission when the conduction band at solid density becomes more atomiclike as energy is transferred from the electrons to the ions. This allows one to determine, independent of plasma simulations, the electron temperature and density just after the decay of crystalline order and to characterize the early time evolution.

DOI: 10.1103/PhysRevLett.106.164801 PACS numbers: 41.60.Cr, 32.30.−r, 32.80.Hd, 32.80.Zb

The rapid heating of solids is of great interest for research in the fields of plasma physics [1], warm dense matter [2], fusion sciences [3], and planetary and astrophysical sciences [4,5]. Theoretically, matter in this state is difficult to address due to the electrostatic and thermal energies being of equivalent importance so that perturbative approaches of either solid-state or classical-plasma physics cannot be applied. Furthermore, it is difficult to obtain quantitative experimental data in this regime. A promising way forward is to use the newly developed

extreme ultraviolet (XUV) and x-ray free electron lasers (XUV/x-ray FELs) to irradiate solid samples [2,6,7]. In the creation of warm dense matter with short-pulse energy sources, such as short-pulse optical lasers, proton beams, and XUV and x-ray FELs, three critical aspects need to be addressed: the first is the uniformity of the energy deposition; the second is the redistribution of the deposited energy among the various degrees of freedom, i.e., the rates of equilibration; and the third is the subsequent response of the warm dense matter.

Using XUV/x-ray FELs the initial energy deposition mechanism via photoionization of inner-shell electrons is well understood, which is in contrast to the use of optical lasers where absorption at critical density dominates. For the XUV and x-ray lasers the frequency of incident photons is much higher than the plasma frequency of the solid, and as the photon energy is also greater than the binding energy of internal shells, absorption of the FEL light occurs via photoabsorption at solid density. It has also been noted that at sufficiently high intensities saturation of this absorption mechanism may guarantee rather uniform samples of warm dense matter [8].

However, as the energy deposition occurs on a 10-fs time scale and is thus much faster than any hydrodynamic motion, the equilibration of the system is an urgent subject of research. We report here measurements of XUV emission providing information on the state of the near solid-density plasma. In particular, we observe at the onset of expansion and plasma densities just below that of a solid the formation of discrete atomic states from out of the conduction band.

The experiment was performed at the FLASH XUV free-electron-laser facility at DESY in Germany. The experimental setup is shown in Fig. 1. Solid Al foils were irradiated at 5 Hz with intense pulses of 13.5 nm radiation (92 eV). Pulses of ~20-fs duration in a 3 mm aperture limited beam size were focused by means of a multilayer-coated (Mo-Si) off-axis parabola with a focal length of 269 mm. The focal spot size was established by analyzing the craters resulting from ablation of poly(methyl methacrylate) (PMMA) for different target positions and pulse energies [9]: at best focus a FWHM of ~2.3 μm was measured. The reflectivity of the parabola was measured after the experiment and found to be 48%. The pulse energies on target varied between 5 and 10 μJ, thus providing maximum intensities of 10^{16} W/cm^2. The primary spectrometer, a Hitachi 1200 lines/mm variable line spacing grating creates a flat spectral focal plane on a CCD camera covering a spectral range from 10 to 30 nm. The harmonic efficiency of the grating in 2nd (3rd) order is 9.5% (2.7%), and is equal to 1.9% (1.8%) of the efficiency of 1st order at wavelengths between 11.8 nm and 18.2 nm, respectively [10]. An Al edge filter was used to determine a spectral resolution ~0.1 nm. Additional shielding (represented by the direct block in Fig. 1) avoids direct emissions from the sample. The samples were composed of 10 μm thick Al foils that were continuously moved transverse to the FEL beam to expose a fresh surface to each FEL pulse.

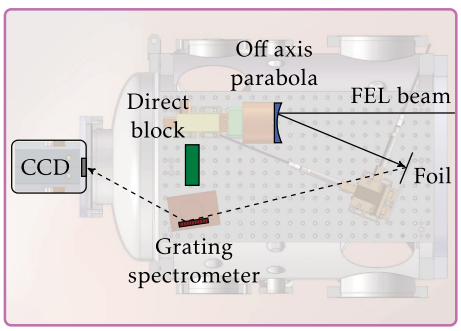

FIG. 1 (color online). A schematic of the experimental layout.

The high photon fluxes create experimental conditions that are distinctly different from those created at synchrotrons, where photoionization of core electrons and associated x-ray transitions have also been studied [11,12]. The difference is due to the multifold increase in spectral brightness resulting in an L-shell electron being excited in almost every atom in the focal spot of the beam simultaneously. The resultant energy density deposition and heating of the sample leads to further core-hole transitions at solid density not observable in the synchrotron case, as well as characteristic emission from the dense plasma formed as the solid-density system later expands.

Figure 2 shows an experimental spectrum with the background subtracted obtained by integrating 2000 shots at best focus. We first identify the ionization stages and configurations from which these lines originate, before discussing their diagnostic of the heating and subsequent expansion of the target. The dominant spectral features are identified by comparison with transition energies obtained from Hartree-Fock calculations [13] as the Al IV lines:

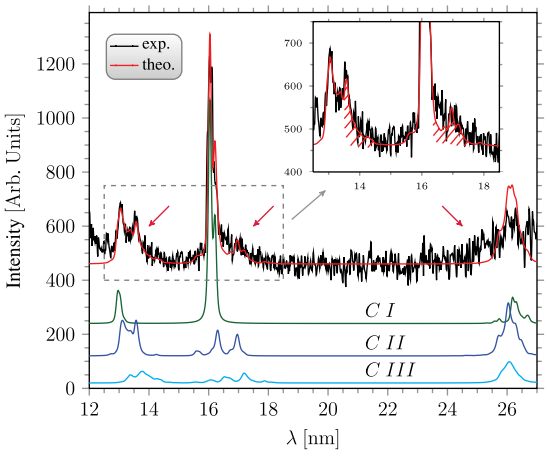

FIG. 2 (color online). Emission spectra (black line) taken at best focus. The arrows indicate the discrepancy between the data and simulation of the Al IV emission (CI). The overlaying (red) curve is the best fit obtained including also the emission from the L-hole states (CII and CIII). The genetic algorithm identifies CI emission at $T_e = 8$ eV, whereas for the CII, CIII emission $T_e = 25$ eV. Curves CI–CIII are offset for clarity.

$1s^2 2s^2 2p^6$–$1s^2 2s^2 2p^5(^2P^o)3s\ ^1P$ and ^3P at 16.1 nm and 16.2 nm, respectively. The transitions at shorter wavelengths are $1s^2 2s^2 2p^6$–$1s^2 2s^2 2p^5 3d\ ^1P$, ^3P, and ^3D at 13.0 nm, 13.1 nm, and 13.2 nm, respectively. Curve CI in Fig. 2 shows the spectral simulation of the Al IV lines including opacity effects. Direct evidence of optical depth effects is reflected in the intensity ratio of the resolved Al IV lines at 16.1 and 16.2 nm, which in optically thin plasmas is ~10 times smaller than the transition at 16.1 nm. Here we observe a much smaller ratio indicating that the plasma emission occurs in an optically thick medium. Opacity is also responsible for the calculated intensities of the transitions at 13.1 nm and 13.2 nm.

A comparison between the experimental data and the simulation (CI) shows important differences indicated by the arrows in Fig. 2. The spectral features shifted relative to the red of resonance lines and shown as hashed areas in the inset of Fig. 2 can be due to screened transitions. The observed features on the red wavelength wing of the Al IV resonance lines are consistent with transitions into the L shell of heated Al while spectator electrons are present in the M shell:

$$\text{Channel II: } (K^2L^7M^2 \rightarrow K^2L^8M^1 + h\nu_{\text{Al III}}),$$

$$\text{Channel III: } (K^2L^7M^3 \rightarrow K^2L^8M^2 + h\nu_{\text{Al II}}).$$

In this notation the unscreened transitions are given by

$$\text{Channel I: } (K^2L^7M^1 \rightarrow K^2L^8M^0 + h\nu_{\text{Al IV}}).$$

Figure 2 shows the spectral calculations and also the individual contributions (CI, CII, CIII) originating from the configurations from doubly ionized Al III, $\alpha = K^2L^7M^2$, and singly ionized Al II, $\beta = K^2L^7M^3$. The spectral distributions have been calculated with the MARIA code [14,15]. The cumulated spectra in Fig. 2 indicated as "theo." demonstrates that the experimental spectra can be well described by the sum of channels I–III. The MARIA calculations identify two strong emission features at 14 nm and 17 nm whose ratio is strongly dependent on the assumed electron temperature, T_e. Using a genetic algorithm that varied the intensity, wavelength shifts of each configuration, and the linear background corrections, we derive the electron temperature T_e. The best fit to the experimental spectrum gives a T_e of 25 ± 10 eV. The uncertainty of this estimate is mainly due to the calibration of the spectrometer, the components of which (grating, CCD) have responses that are frequency dependent. This electron temperature is *inconsistent* with simple inner-shell photoionization: after photoionization of almost every atom during the 20-fs XUV pulse, an excess energy of ~19 eV will be distributed among the 4 electrons in the conduction (M) band. Assuming sub-fs-scale thermalization [16] of the excited electrons with the original 3 electrons in the conduction band ($\epsilon_F = 11.6$ eV), a T_e^{PI} of ~7 eV is expected. We note that the electron temperature of $T_e = 8$ eV deduced from the Al IV emission (Fig. 2) is further confirmation that the T_e^{PI} is inconsistent with simple photoionization.

In order to develop a consistent picture for the XUV emission, we next consider estimates of the electron density. In the high-density limit, the population ratio of the autoionizing levels α' and β' (being single levels of the configurations α and β) is given by

$$\frac{n^{\text{II}}_{\beta'}}{n^{\text{III}}_{\alpha'}} \approx n_e \frac{g^{\text{II}}_{\beta'}}{g^{\text{III}}_{\alpha'}} \left(\frac{2^{1/3}\pi\hbar^2}{m_e k_B T_e}\right)^{3/2} e^{(-\Delta E_{\alpha'\beta'}/k_B T_e)}. \quad (1)$$

$\Delta E_{\alpha'\beta'}$ is the energy difference between α' and β', and $g^{\text{II}}_{\beta'}$, $g^{\text{III}}_{\alpha'}$ are the statistical weights. We note that changes in the ionization potential due to the dense strongly coupled plasma environment are expected to be small as Eq. (1) contains only energy differences. Using a genetic algorithm we were able to extract the population ratio $n^{\text{II}}_{\beta'}/n^{\text{III}}_{\alpha'}$ because the ratio of different spectral partition functions is almost constant. Assuming the high-density limit to be valid, Eq. (1) provides the electron density: $n_e = 10^{22}$–10^{23} cm^{-3}, i.e., a significant fraction of n_e at solid density, where the n_e in the conduction band is 1.8×10^{23} cm^{-3}. Stark broadening calculations carried out with PPP code [17] seem to be in agreement with the densities; also Stark transitions do not change much the spectral functions.

These high densities inferred are consistent with an analysis which employs the characteristic time scales for the relevant processes. It shows there is a substantial difference in the temporal evolution of autoionizing configurations (α, β) and nonautoionizing ones. Since transition probabilities of Al IV lines are 10^9 to 10^{11} s^{-1} [13], the self-emission occurs about 0.1 ns after excitation, which is much longer than the 20-fs FEL pulse. Therefore, this emission corresponds to times well after the pulse. In contrast, the situation for the channels II and III is radically different because configurations α and β are autoionizing with time that scales inversely with Auger rates, i.e., $1/\Gamma_{\alpha\beta,\gamma}$ ($\gamma = K^2L^8M^{0,1}$) being ≤ 100 fs [13]. As radiative decay times are orders of magnitudes longer, the observed radiative emission has a time scale that is essentially determined by autoionization rather than by radiative decay [18]:

$$\tau_{\text{II,III}} \approx \frac{1}{\sum A + \sum \Gamma} \approx \frac{1}{\sum \Gamma}. \quad (2)$$

The principle of microreversibility relates the Auger rate $\Gamma_{\alpha\beta,\gamma}$ to its inverse rate coefficient $\Gamma^{\text{inv}}_{\alpha\beta,\gamma}$:

$$g_\gamma \Gamma^{\text{inv}}_{\alpha\beta,\gamma} = g_{\alpha\beta}\Gamma_{\alpha\beta,\gamma}\left(\frac{2^{1/3}\pi\hbar^2}{m_e k_B T_e}\right)^{3/2} e^{(-E_{\alpha\beta,\gamma}/k_B T_e)}. \quad (3)$$

The above argument provides a consistent picture for the time evolution as the inverse Auger effect is important for the emission from channels II and III. As the electron

temperature of 25 eV (Fig. 2) is of the same order as the capture energy $E_{\alpha\beta,\gamma}$, Eq. (3) indicates that the inverse processes are effective.

This has two important implications. First, since direct and inverse processes are related by first principles, the inverse processes are indicative of the evolution phase of the system right after the disassembly of the target. Second, the inverse process can directly induce $2s$ and $2p$ vacancies ($1s^2 2s^1 2p^6 M^X$ and $1s^2 2s^2 2p^5 M^X$) as well as corresponding intrashell transitions: emission near 26 nm (see Fig. 2). Note that in the present experiment the 92 eV laser photon cannot photoionize the $2s$ electrons and corresponding hole states cannot be produced. Therefore, the transitions $1s^2 2s^1 2p^6 M^X \rightarrow 1s^2 2s^2 2p^5 M^X + h\nu_{2s\text{-}2p}$ are characteristic intrashell transitions of the inverse Auger effect (also collisional inner-shell excitation might contribute). As Fig. 2 demonstrates, the intrashell transitions are indeed observed. It is important to note that Eq. (3) implies that the emission from hole states (channels II, III, or intrashell) is not sensitive to a radiative recombination regime at low density (and the same holds true for collisional inner-shell excitation). Therefore they are indicators of high density in the early stage of target evolution even in time integrated spectra [19]. Moreover, our calculations show that even the relative intensity of the intrashell transitions near 26 nm is in reasonable agreement compared to those near 13 nm and 16 nm from channels II and III.

All the above reasoning leads us to conclude that channels II, III and corresponding intrashell transitions $2s$-$2p$ will be seen at very high plasma densities. As Eq. (1) indicates, the observed line emission in these channels *does not* come from solid density itself. This is consistent with the fact that under such conditions no discrete atomic states exist in the M band: as the density falls below solid (2.7 g/cm^3), distinct atomic states appear at densities lower than about 2.0 g/cm^3 and the ionization of the M-band electrons leads to different ionization stages. We therefore associate the electron temperature T_e and density n_e deduced from channels II and III to the time interval that occurs in the early time expansion phase of the target, i.e., about 3.5 ps. This time scale after FEL irradiation will be affected by the electron-ion coupling time, which is thought to be greater than a ps for these conditions [20].

The spectroscopically deduced temperature of 25 eV from channels II and III is consistent with Auger heating. As discussed above, after photoionization of almost every atom a T_e^{PI} of $\sim$7 eV is expected. The fluorescence yield of this excited transient state is 0.02, and thus the vast majority of excited states decay by Auger effect. Assuming that the Auger electron energy of 70 eV (e.g., equivalent to the energy difference between the configurations $K^2L^8M^3$ and $K^2L^7M^4$ [13]) rapidly thermalizes with the three remaining 7 eV electrons in the conduction band yields a T_e of $\sim$30 eV.

Moreover, as indicated in Fig. 2 the genetic algorithm predicts Al IV emission (channel I) at $T_e = 8$ eV. This corresponds to the later expansion phase where electron cooling due to ionization of the M electrons has become important.

In conclusion we have characterized independent of plasma simulations important steps in the sub-ps evolution and equilibration of matter via the subsequent production of multiple hole states: first, $2p$-hole states are produced by photoionization of the cold solid when high intensity short-pulse XUV free-electron-laser radiation interacts with solid matter. The hole states decay via Auger effect on a time scale of about 40 fs, whereas the Auger electrons lead to a rapid heating of the conduction band electrons. A subsequent decay of crystalline order on a ps time scale accompanied by the inverse Auger effect efficiently creates hole states in the $2s$ and $2p$ shells and thus leads to the characteristic features in the spectral emission of hole states when the crystalline order has just decayed.

*Also at École Polytechnique, LULI, PAPD, 91128 Palaiseau, France
†frank.rosmej@upmc.fr

[1] R. Davidson, *Frontiers in High Energy Density Physics: The X-Games of Contemporary Science* (National Academies Press, Washington, DC, 2003).
[2] R. W. Lee *et al.*, J. Opt. Soc. Am. B **20**, 770 (2003).
[3] J. D. Lindl *et al.*, Phys. Plasmas **11**, 339 (2004).
[4] T. Guillot, Science **286**, 72 (1999).
[5] M. Turner, *Connecting Quarks with the Cosmos: Eleven Science Questions for the New Century* (National Academies Press, Washington, DC, 2003).
[6] M. Fajardo *et al.*, Eur. Phys. J. D **29**, 69 (2004).
[7] F. B. Rosmej and R. W. Lee, Europhys. Lett. **77**, 24 001 (2007).
[8] B. Nagler *et al.*, Nature Phys. **5**, 693 (2009).
[9] A. J. Nelson *et al.*, Opt. Express **17**, 18 271 (2009).
[10] D. Neely, Ph.D. thesis, Queen's University Belfast, 1992.
[11] S. Flügge, *Handbuch der Physik* (Springer, New York, 1955).
[12] J. M. Ziman, *Principles of the Theory of Solids* (Cambridge University Press, London, 1972).
[13] R. D. Cowan, *The Theory of Atomic Structure and Spectra* (University of California Press, Berkeley, 1980).
[14] F. B. Rosmej, J. Phys. B **30**, L819 (1997).
[15] F. B. Rosmej, Europhys. Lett. **76**, 1081 (2006).
[16] W. S. Fann, R. Storz, H. W. K. Tom, and J. Bokor, Phys. Rev. B **46**, 13 592 (1992).
[17] A. Calisti, B. Talin, C. Mosse, and S. Ferri (private communication).
[18] F. B. Rosmej, in *Highly Charged Ions* edited by R. Hutton *et al.* (Taylor and Francis, London, 2010).
[19] F. B. Rosmej, R. W. Lee, and D. H. G. Schneider, High Energy Density Phys. **3**, 218 (2007).
[20] B. Rethfeld *et al.*, Phys. Rev. B **65**, 214303 (2002).